Progress In Electromagnetics Research M, Vol. 106, 191–203, 2021

Compensation Rotor Vibration of Outer Rotor Coreless Bearingless Permanent Magnet Synchronous Generator Using Variable Step Least Mean Square Adaptive Filter

Huangqiu Zhu, Kai Zhou*, and Junqi Huan

Abstract—An outer rotor coreless bearingless permanent magnet synchronous generator (ORC-BPMSG) has the characteristics of long service life, high efficiency, low noise, etc. However, the stability and reliability of the system and the output voltage are affected by the rotor vibration. In this paper, the step size and error of improved variable step least mean square (VSLMS) adaptive filter using improved simplified particle swarm optimization (ISPSO) is proposed, which suppresses the vibration of the rotor. The mathematical model and working principle of the ORC-BPMSG are introduced. The performances of improved VSLMS adaptive filter parameters are optimized by the ISPSO algorithm, which generates a compensation signal to realize vibration compensation. The simulation system for the vibration compensation of the ORC-BPMSG is constructed, and dynamic suspension experiment and variable speed experiment of the rotor are carried out, which verify the robustness and stability of the proposed method.

1. INTRODUCTION

With the deterioration of the global environment and the depletion of oil resources, there is an urgent need to develop and popularize new energy sources and their applied technologies. Permanent magnet synchronous generator (PMSG) has been widely used in many occasions, such as wind turbine, gas turbine, hybrid vehicle, and flywheel energy storage system electric power generation integrated machine, because of its advantages of simple structure, small volume, high efficiency, low loss, reliable operation, and high power factor [1–4]. Therefore, the stable operation of the generator is very important. In order to reduce the impact of bearing wear and stator core loss, an ORC-BPMSG is proposed in this paper. Compared with traditional generators, the outer rotor coreless bearingless generator has the advantages of no contact, no wear, low maintenance cost, and high reliability, and can achieve high speed and high precision [5–8]. However, in the process of motor production and manufacture, the rotor mass eccentricity is caused by the lack of machining accuracy, which makes the rotor produce a large eccentricity force at high speed rotation, thus causing the unbalanced vibration of the rotor. When the rotational speed reaches a certain value, the eccentric displacement of the rotor may exceed the air gap of the motor, resulting in collision and friction of the stator and rotor [9, 10]. During the vibration of the suspended rotor of the stator coreless bearingless generator, the uneven distribution of the air gap magnetic density leads to the fluctuation of the voltage emitted by the generator and the decrease of the power quality [11]. Aiming at the problem of rotor unbalanced vibration, a variety of vibration compensation methods have been put forward. [12] proposes feed-forward decoupling control to suppress rotor unbalanced vibration; however, it is necessary to utilize an optimal tracking differentiator to obtain compensation, which makes reliability and stability decrease. In [13], a variable step size real time iterative optimization algorithm which is used to compensate the imbalance of the

Received 5 October 2021, Accepted 16 December 2021, Scheduled 24 December 2021
* Corresponding author: Kai Zhou (1315852003@qq.com).
The authors are with the School of Electrical and Information Engineering, Jiangsu University, Zhenjiang 212013, China.

active magnetic bearing rotor system is proposed. However, convergence reliability is not high during the iterative solution. In [14], a new type of frequency estimation adaptive notch filter based on active magnetic bearings which eliminate synchronous current is proposed. However, the convergence of the adaptive notch filter algorithm is affected by the closed loop of active magnetic bearings systems. In [15], a control strategy that integrates feed-forward compensation and current compensation for radial offset and unbalanced vibration caused by uneven rotor mass is proposed, but vibration compensation can only achieve better results in low speed. To improve the reliability and stability of compensation, a variable step least mean square adaptive filter based on improved simplified particle swarm optimization (ISPSO) algorithm is proposed. This algorithm can reliably converge and has a rapid response speed stably at high speed. By Matlab/Simulink simulation, the effectiveness and stability of the proposed method are verified.

2. OPERATION PRINCIPLE AND MATHEMATICAL

The ORC-BPMSG is based on the permanent magnet synchronous generator. A set of suspension windings is added to the stator, and ORC-BPMSG is shown in Fig. 1. The pole pair number of the generating windings is defined as P_{G}, and the pole pair number of the suspension windings is defined as P_{B}. If the relationship between the number of pole pairs of the two sets of windings is $P_{\mathrm{G}} = P_{\mathrm{B}} \pm 1$, a radial controllable levitation force can be generated [16].

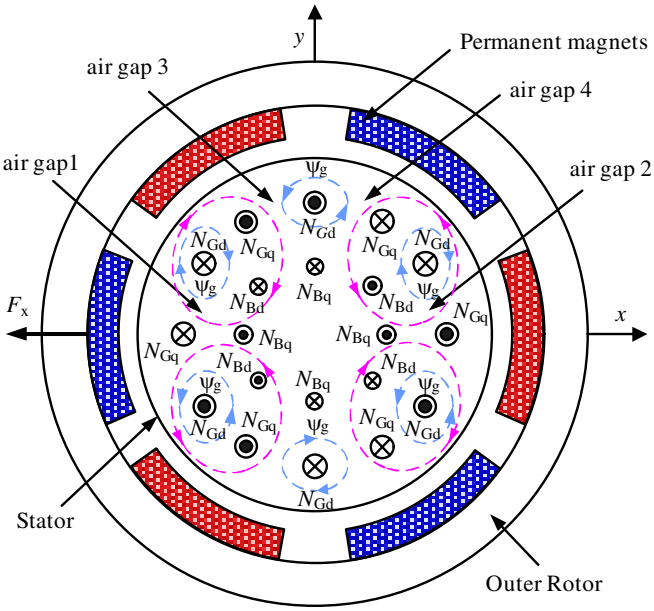

Figure 1. Schematic diagram of suspension force generation.

In Fig. 1, $P_{\mathrm{G}} = 3$, $P_{\mathrm{B}} = 2$, when the generator is driven to rotate by the prime mover, the magnetic induction lines are cut, and the induced current is formed in the generating windings, which produces a symmetrically distributed six-pole magnetic link. When the currents are injected into the suspension windings, the symmetrical distribution of the four-pole magnetic link are generated. When the two magnetic fields are superimposed, the magnetic fields at air gap 1 and air gap 3 are strengthened, and the magnetic fields at air gap 2 and air gap 4 are weakened. The unbalanced air gap magnetic density produces a radial suspension force F_x in the negative direction of the x-axis. The radial suspension force in the other directions can be obtained by changing the direction of the current in the windings.

The ORC-BPMSG needs to use power electronic technology to stabilize the output voltage and constant frequency during the power generation process. The three-phase controllable PWM rectifier circuit is shown in Fig. 2, which is used to convert the obtained alternating current with unstable frequency into direct current and to control the output voltage of the generator.

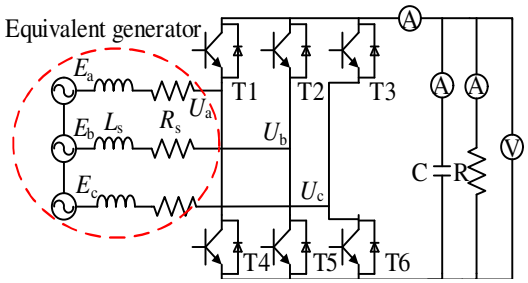

Figure 2. PWM rectifier circuit.

The three-phase flux equation of ORC-BPMSG is

$$\begin{cases} \psi_{\mathrm{a}} = -L_{\mathrm{a}} i_{\mathrm{a}} - M_{\mathrm{ab}} i_{\mathrm{b}} - M_{\mathrm{ac}} i_{\mathrm{c}} + \psi_{\mathrm{af}} \\ \psi_{\mathrm{b}} = -L_{\mathrm{b}} i_{\mathrm{b}} - M_{\mathrm{ba}} i_{\mathrm{a}} - M_{\mathrm{bc}} i_{\mathrm{c}} + \psi_{\mathrm{bf}} \\ \psi_{\mathrm{c}} = -L_{\mathrm{c}} i_{\mathrm{c}} - M_{\mathrm{ca}} i_{\mathrm{a}} - M_{\mathrm{cb}} i_{\mathrm{b}} + \psi_{\mathrm{cf}} \end{cases} \tag{1}$$

where ψ_{a}, ψ_{b}, ψ_{c} are three-phase stator flux linkages, respectively; L_{a}, L_{b}, L_{c} are the three-phase stator self-inductances; $L_{\mathrm{a}} = L_{\mathrm{b}} = L_{\mathrm{c}}$, M_{ab}, M_{ac}, M_{ba}, M_{bc}, M_{ca}, M_{cb} are the mutual inductances between the windings of each phase; and $M_{\mathrm{ab}} = M_{\mathrm{ac}} = M_{\mathrm{ba}} = M_{\mathrm{bc}} = M_{\mathrm{ca}} = M_{\mathrm{cb}}$, ψ_{af}, ψ_{bf}, ψ_{cf} are the flux linkages generated by the rotor in the stator magnetic field. According to the flux linkage equation, the voltage equation is

$$\begin{cases} u_{\mathrm{sd}} = R_{\mathrm{s}} i_{\mathrm{sd}} - \omega_{\mathrm{r}} \psi_{\mathrm{sq}} + \dfrac{\mathrm{d}\psi_{\mathrm{sd}}}{\mathrm{d}t} \\ u_{\mathrm{sq}} = R_{\mathrm{s}} i_{\mathrm{sq}} - \omega_{\mathrm{r}} \psi_{\mathrm{sd}} + \dfrac{\mathrm{d}\psi_{\mathrm{sq}}}{\mathrm{d}t} \end{cases} \tag{2}$$

where R_{s} is the stator windings resistance, and ω_{r} is the rotation speed.

According to the Maxwell tensor method, the expression of the radial suspension force of the ORC-BPMSG in the synchronous rotating coordinate system can be expressed as:

$$\begin{cases} F_{\mathrm{x}} = (k_{\mathrm{G}} - k_{\mathrm{L}})(i_{\mathrm{Bd}} \psi_{\mathrm{Gd}} + i_{\mathrm{Bq}} \psi_{\mathrm{Gq}}) + k_{\mathrm{c}} x \\ F_{\mathrm{y}} = (k_{\mathrm{G}} + k_{\mathrm{L}})(i_{\mathrm{Bq}} \psi_{\mathrm{Gd}} - i_{\mathrm{Bd}} \psi_{\mathrm{Gq}}) + k_{\mathrm{c}} y \end{cases} \tag{3}$$

where $k_{\mathrm{G}} = \frac{\pi P_{\mathrm{B}} P_{\mathrm{G}} L_{\mathrm{B}}}{8 l r \mu_0 N_1 N_2}$, $k_{\mathrm{L}} = \frac{m_{\mathrm{t}} P_{\mathrm{G}} N_2}{4 r P_{\mathrm{B}} N_1}$, $k_{\mathrm{C}} = \frac{\pi P_{\mathrm{G}}^2 \hat{\psi}_{\mathrm{G}}^2}{8 l r \mu_0 N_1^2 \delta_0}$; l is the length of the rotor core; r is the rotor radius; μ_0 is the vacuum permeability; L_{B} is the self-inductance of the suspension windings; N_1, N_2 are the number of turns of power generation and suspension windings; P_{G} is the pole pair number of genereting windings; P_{B} is the pole pair number of suspension windings; m_{t} is the number of motor phases; $\hat{\psi}_{\mathrm{G}}$ is the amplitude of the air gap flux linkage of each phase of the genereting windings. δ_0 is the air gap length; i_{Gd} and i_{Gd}, ψ_{Gd}, and ψ_{Gd} are the d-q axis components of the suspension windings current and the torque windings synthesis air gap flux linkage.

3. DESIGN OF CONTROLLER

3.1. Unbalanced Vibration Analysis

When the rotor vibration of generator is compensated, the unbalanced vibration of generator rotor needs to be analyzed. Normally, the rotor geometric center of the generator is taken as the equilibrium position. When the rotor does not have mass eccentricity and the rotor rotates away from the geometric center, the signal will be fed back, and the current and direction of the suspension windings are adjusted by the PID controller to make the rotor return to the equilibrium position.

Due to machining accuracy and other reasons, the rotor will have mass eccentricity when rotating. The center of inertia O and geometric center O' are not at the same position in Fig. 3. The eccentric displacement of the rotor is e. When the rotor speed becomes faster, the vibration becomes bigger, and the displacement of the rotor also increases. The reliability and stability of the system are seriously

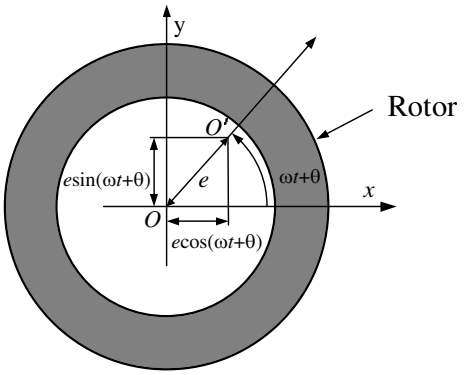

Figure 3. Rotor eccentricity diagram.

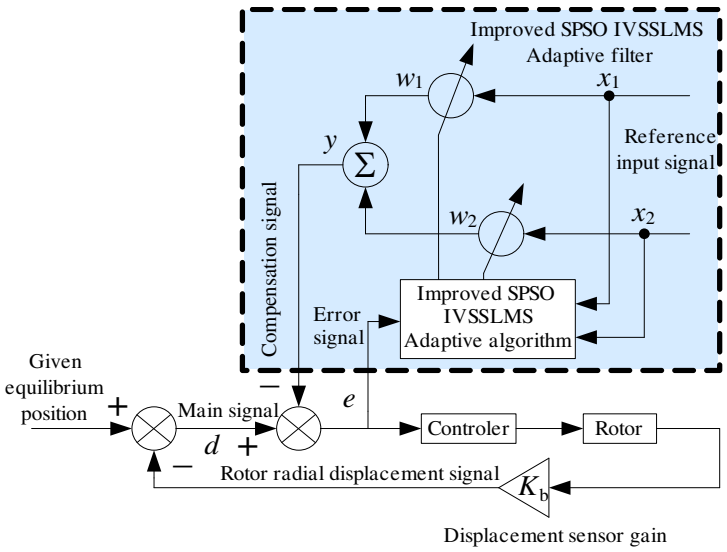

Figure 4. Control block diagram of rotor radial displacement of adaptive LMS filter.

affected. As shown in Fig. 4, when the rotor rotates around the central axis at an angular velocity ω, the centrifugal force on the rotor will be changed with the position of the rotor.

Uncertain displacement is expressed as γ_{b}, and the vibration displacement which is expressed as γ_{s} is at the same frequency, then the radial displacement γ can be written as

$$\gamma = \gamma_{\mathrm{b}} + \gamma_{\mathrm{s}} \tag{4}$$

where $\gamma_{\mathrm{s}} = A_0 \cos(\omega \mathrm{t} + \varphi)$; A_0 is the amplitude of the vibration displacement at the same frequency as the rotor.

The centrifugal force on the rotor is proportional to the square of the speed. Therefore, when the speed is higher, the unbalanced vibration will be more severe. In severe cases, the normal operation and stability characteristics of the motor suspension system will be affected. If the force is not compensated and controlled, the rotation accuracy of the rotor will be greatly affected. If the same-frequency vibration signal γ_{s} in the displacement signal γ in the above formula can be removed by filtering or cancellation, the control signal that generates the periodic control force can be eliminated before entering the PID controller. Therefore, the feed-forward compensation based on an improved VSLMS adaptive filter is used. The vibration signal with the same frequency as the rotational speed can be extracted from the radial displacement sensor. Then according to the improved variable step size LMS algorithm, the adaptive weight coefficient is adjusted to generate a sinusoidal compensation signal, and the vibration signal is compensated.

3.2. Compensation Control of Unbalanced Vibration Design of Adaptive Filter Based on Improved Variable Step LMS Algorithm

The designed improved variable step size LMS adaptive filter is added to the radial displacement control of the suspended rotor, and the control block diagram is shown in Fig. 4.

The main signal d is composed of uncertain displacement signal d_{a} and rotor mass radial eccentric displacement signal d_{s} with the same frequency as the speed. The reference input signals x_1 and x_2 are respectively sine and cosine signals with the same frequency as the rotational speed. The adaptive parameters are adjusted by LMS algorithm w_1, w_2, and compensation signal y is output which is weighted by two reference input signals. This signal is used as a feedback compensation signal, which is always equal to the rotor radial displacement amplitude. The phase of signal is same as the vibration signal, and the direction of signal is opposite to vibration signal. Then the error signal e of the main signal d and compensation signal y are input into the algorithm, and the iterative operation is performed to output an accurate compensation signal that can compensate the radial displacement of the rotor. In Fig. 4, the expression of the main signal composed of the random displacement and radial displacement of the rotor is

$$d(nT) = d_{\mathrm{a}}(nT) + A\cos(n\omega T + \theta) \tag{5}$$

where T is the sampling period, A the rotor displacement signal amplitude, ω the rotor angular frequency, and θ the initial phase angle of the rotor.

The expression of the reference input signal $X(nT)$ is

$$X(naT) = \begin{bmatrix} x_1(nT) \\ x_2(nT) \end{bmatrix} = A \begin{bmatrix} \sin(n\omega T + \phi) \\ \cos(n\omega T + \phi) \end{bmatrix} \tag{6}$$

In the LMS algorithm, the expressions of the two weight coefficients w_1 and w_2 are

$$\begin{cases} w_1(n+1) = w_1(n) + 2\mu(n)e(n)x_1(n) \\ w_2(n+1) = w_2(n) + 2\mu(n)e(n)x_2(n) \\ e(n) = d(n) - y(n) \\ y(n) = w_1(n)x_1(n) + w_2(n)x_2(n) \end{cases} \tag{7}$$

In the traditional LMS algorithm, when the value of the step size factor $\mu(n)$ is large, the convergence speed can be achieved. However, the steady-state error is relatively large. When the step size factor is small, a small steady-state error can be obtained, but the convergence speed is slower. Therefore, the step size is constantly changed by the variable step size LMS algorithm during the convergence process. On this basis, the nonlinear relationship between the step size factor and the error signal is introduced, and the constant value parameters in the algorithm are replaced with new parametric function expressions. The improved nonlinear function model is

$$\mu(n) = \beta(n)\left[\frac{1}{4} - \frac{\exp(-\alpha(n))}{(1+\exp(-\alpha(n)))^2}\right] \tag{8}$$

$$\alpha(n) = \eta\,|e(n)e(n-1)|^m \tag{9}$$

$$\beta(n) = p\beta(n-1) + \lambda e^2(n) \tag{10}$$

where η, m, p, and λ are constant value parameters, which jointly control the performance of the algorithm among which $\eta > 0$, $m > 0$, $0 < p < 1$, and $0 < \lambda < 1$. When the error decreases, the parametric functions $\alpha(n)$ and $\beta(n)$ decrease, and the step size decreases accordingly. Therefore, the ISPSO algorithm is used to optimize the constant value parameters.

3.3. Improved Particle Swarm Algorithm to Optimize Filter

The particle swarm optimization (PSO) algorithm is used to search for the optimal solution in the space, and the position and velocity of each particle need to be iterated and updated during the implementation of the algorithm. The update formula of the velocity v_{id} and position x_{id} of the i-th particle in the d dimensional space in the standard PSO algorithm can be expressed as:

$$\begin{cases} v_{id}(t+1) = wv_{id}(t) + c_1r_1[p_{id}(t) - x_{id}(t)] + c_2r_2[p_{gd}(t) - x_{id}(t)] \\ x_{id}(t+1) = x_{id}(t) + v_{id}(t+1) \end{cases} \tag{11}$$

where w is the inertia weight; $c_1 = c_2 = 2$ are the learning factors; r_1 and r_2 are randomly distributed in $[0, 1]$; t is the number of iterations; $i = 1, 2, \ldots, Np$, Np is the population size; $p_i = (p_{i1}, p_{i2}, \ldots, p_{id})$ is the individual optimal position; and p_g is the global optimal position.

In order to solve the problem that the PSO algorithm is easy to fall into the local optimum, and the local search ability increases with the decrease of the inertia weight, while the global search ability is the opposite, the ISPSO algorithm that improves the inertia weight and learning factor is proposed. This method combines the linear differential reduction strategy and dynamic change strategy. When the influence degree of the two strategies in the inertia weight changes, the learning factor also changes, and the global and local search capabilities of the ISPSO algorithm also change. ISPSO position update formula of the algorithm can be expressed as:

$$x_i(t+1) = wx_i(t) + c_1r_1[p_i(t) - x_i(t)] + c_2r_2[p_g(t) - x_i(t)] \tag{12}$$

$$x_i(t+1) = wx_i(t) + c_1r_1\left[\frac{p_i(t) + p_g(t)}{2} - x_i(t)\right] + c_2r_2\left[\frac{p_i(t) - p_g(t)}{2} - x_i(t)\right] \tag{13}$$

The calculation formula of the linear differential decline strategy is

$$\frac{dw}{dt} = \frac{2(w_{\max} - w_{\min})}{T_{\max}^2}t \tag{14}$$

$$\int_{w(t)}^{w_{\max}} dw = \frac{2(w_{\max} - w_{\min})}{T_{\max}^2}\int_0^t \tau d\tau \tag{15}$$

$$w_1(t) = w_{\max} - \frac{w_{\max} - w_{\min}}{T_{\max}^2} \cdot t^2 \tag{16}$$

where $w_{\max} = 0.9$; $w_{\min} = 0.4$; $T = 100$ is the maximum number of iterations.

The dynamic change strategy calculation formula is

$$w_2(t) = \left(\frac{w_{\max} - w_{\min}}{2}\right)\cos\left(\frac{\pi t}{T}\right) + \frac{w_{\max} + w_{\min}}{2} \tag{17}$$

where $w_{\max}$ and $w_{\min}$ are the maximum values of the inertia weight w, taking the values 0.9 and 0.4, respectively.

Combining the above two inertia weighting strategies, namely Equations (16) and (17) linearly, a mixed strategy of inertia weights is obtained, which can be expressed as

$$w(t) = \lambda_1 w_1(t) + \lambda_2 w_2(t) \tag{18}$$

where $0 \le w_1 \le 1$, $0 \le w_2 \le 1$, $w_1 + w_2 = 1$, the degree of influence of the classic two changing strategies on the inertia weight w can be controlled by changing the values of w_1 and w_2.

The calculation formula of the learning factor is

$$\begin{cases} c_1(t) = 0.5w^2(t) + w(t) + 0.5 \\ c_2(t) = 2.5 + 2.2w(t) - c_1(t) \end{cases} \tag{19}$$

3.4. The Model of LMS Adaptive Filter Based on ISPSO Optimization and Improved Variable Step Size

The compensation performance of the improved variable step size LMS adaptive notch filter largely depends on the values of the parameters η, m, p, λ in the improved variable step size model. Therefore, the optimization of parameters is particularly significant. In order to realize the compensation of rotor vibration, this paper adopts the ISPSO algorithm to optimize the performance parameters η, m, p, λ so that the filter achieves the best compensation effect.

Determine the reference input signal x_1, x_2. The main signal d is calculated by radial displacement signal detection, and the performance parameters of the variable step size LMS adaptive filter are optimized by the ISPSO. The specific steps are as follows.

Initialization. The parameters of the algorithm are given initial values. The population size is $N_p = 20$; the maximum number of iterations is $T = 100$; and the values of $w_{\max}$ and $w_{\min}$ are taken as

0.9 and 0.4, respectively. The particle swarm is initialized randomly, according to the initial position of the particle. The initial value of the parameter can be calculated according to Equation (7).

Judge the pros and cons of the particles. The mean square error of the error and the step size are taken as the fitness function of the ISPSO algorithm, and the expression is

$$F = \frac{1}{N_p} \sum_{i=1}^{N} |e_i - \mu_i|^2 \tag{20}$$

where e_i is the error signal, and μ_i is the step size. The fitness value of each particle is calculated according to Eq. (20).

Update the particle position. According to Eq. (13), the particle position is updated to produce the next generation of particles. The expression is

$$\begin{aligned} x_k(t+1) \;=\; & \left[\lambda_1 \left(0.9 - \frac{0.5}{10000} t^2\right) + (1-\lambda_1)\left(\frac{0.5}{2}\cos\frac{\pi t}{100} + \frac{1.3}{2}\right)\right] x_k(t) \\ & + c_1(t) r_1 \left[\frac{p_k(t) + p_g(t)}{2} - x_k(t)\right] + c_2(t) r_2 \left[\frac{p_k(t) - p_g(t)}{2} - x_k(t)\right] \end{aligned} \tag{21}$$

Determine whether to terminate the iteration. If the calculation result of formula (20) is less than the requirement of convergence accuracy or the current iteration number has reached the maximum number of iterations, the iteration is terminated and the result is output otherwise, let $t = t + 1$, and go to step 2).

In this way, the rotor unbalance vibration compensation can be performed from the detected displacement signal. In order to make the filter achieve the best prediction effect, the ISPSO algorithm is used to optimize the performance parameters and obtain the optimal parameters $(\eta, m, p, \lambda) = (100, 1.5, 0.95, 0.01)$.

4. EXPERIMENTAL TEST

The control system of ORC-BPMSG is mainly composed of two parts: output voltage control and radial suspension force control. The ISPSO improved VSLMS adaptive filter is included in the radial suspension force control system. The controllable rectifier circuit with the thyristor is used to rectify the output voltage, and an ISPSO improved VSLMS adaptive filter is used to generate a set of compensation signals λ_x and λ_y with the same frequency as the speed for the control of the radial suspension force to cancel the vibration signal component of the radial displacement signal with the same frequency as the speed. Therefore, the signal of the controller does not contain the vibration signal component with the same frequency as the speed, so as to suppress the radial vibration caused by the eccentricity of the rotor mass, and at the same time, the fluctuation of the output voltage can be reduced.

In order to verify the effectiveness of the proposed IVSLMS adaptive filter based on the ISPSO optimization for the rotor vibration compensation of the ORC-BPMSG, a simulation model of the control system is built in the Matlab/Simulink.

The control system block diagram of the ORC-BPMSG is shown in Fig. 5. Since the generator needs to be driven by the prime mover, there are many interference factors in the vibration compensation effect of the rotor during the floating stage, so the experiments and simulations are both carried out in the stable suspension stage. In the simulation, when the given speed reaches 3000 r/min, the rotor vibrates due to the eccentricity of the rotor mass. Fig. 6 is the vibration waveform diagram of the rotor in the x- and y-directions. Without unbalance compensation, the peak values of the radial displacement in the x- and y-directions are maintained at about 35 μm.

Figure 7 is a waveform diagram in the x- and y-directions with compensation. By improving the variable step size LMS adaptive filter compensation, the peak value of the radial displacement is kept within 12 μm. Through the compensation of the improved VSLMS adaptive filter based on the ISPSO optimization, the peak value of the radial displacement is kept within 6 μm, and the vibration compensation effect ratio is optimized. The former is more obvious.

Figure 8(a) is the output voltage when the rotor is not compensated. The output voltage fluctuates greatly after rectification, and the peak-to-peak fluctuation is about 15 V. Fig. 8(b) shows that after

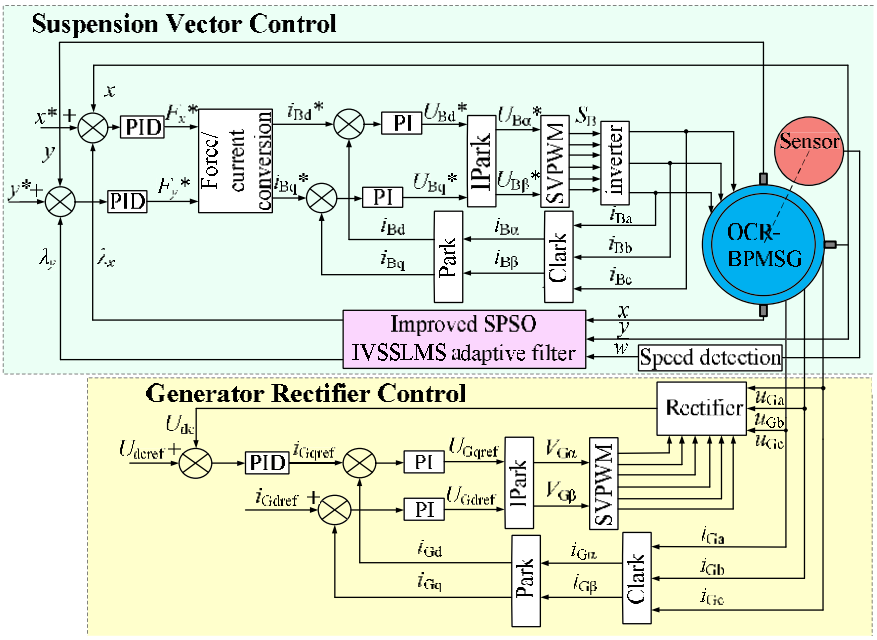

Figure 5. Frame diagram of ORC-BPMSG based on ISPSO Improved VSSLMS model.

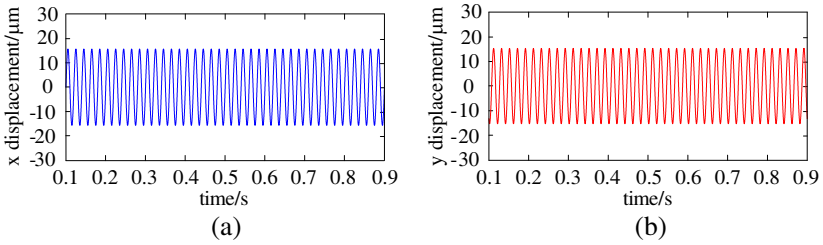

Figure 6. Vibration waveform diagram of the rotor in the (a) x- and (b) y-direction.

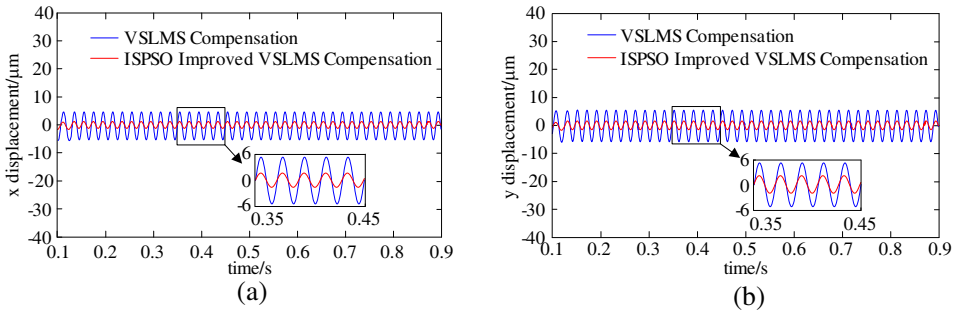

Figure 7. Vibration waveform diagram of the rotor after compensation in the (a) x- and (b) y-direction.

the proposed VSLMS adaptive filter optimization for the rotor vibration compensation, the peak-to-peak value of the output voltage fluctuation of the rotor is about 10 V. Fig. 8(c) is that the output voltage fluctuation of the rotor after the proposed improved VSLMS adaptive filter based on the ISPSO optimization for the rotor vibration compensation is small; the peak-to-peak value of the fluctuation is about 5 V; the rotor suspension performance is better; and the compensation effect is more obvious.

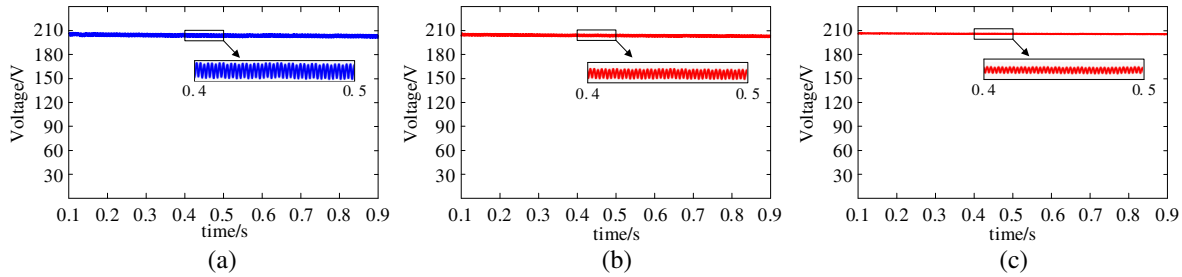

Figure 8. The output voltage of ORC-BPMSG. (a) Uncompensated output voltage. (b) The output voltage after VSLMS compensation. (c) The output voltage after ISPSO improved VSLMS compensation.

5. EXPERIMENTAL VERIFICATION

As shown in Fig. 9(a) is an experimental diagram of the motion trajectory of the uncompensated rotor. Figs. 9(b) and 9(c) are experimental plots of rotor motion trajectories compensated with variable step size LMS adaptive filters and improved VSLMS optimized adaptive filters. After compensation, the motor rotor suspension is more stable, suspended near the origin, and the fluctuation is small. The control strategy in this paper has a good suspension performance.

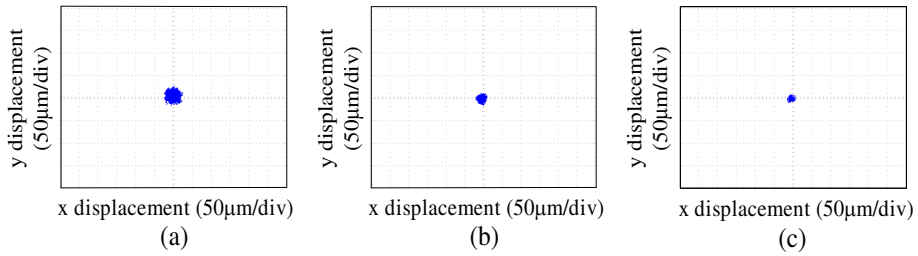

Figure 9. Experiment results of trajectory of the rotor. (a) Uncompensated displacement. (b) The displacement after VSLMS compensation. (c) The displacement after ISPSO improved VSLMS compensation.

Fig. 10(a) and Fig. 10(b) show the curves of rotor radial displacement without compensation and through variable step length LMS adaptive filter compensation. Without compensation, the peak-to-peak value of the rotor radial displacement is about 36 μm.

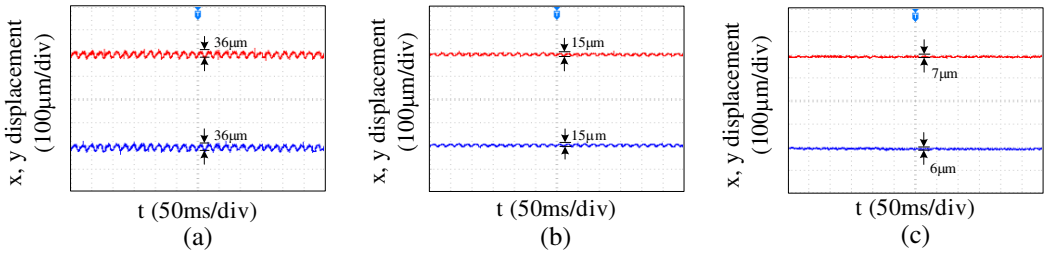

Figure 10. Experiment results of the rotor displacement in the x- and y-direction. (a) Uncompensated displacement. (b) The displacement after VSLMS compensation. (c) The displacement after ISPSO improved VSLMS compensation.

After compensation by the variable-step LMS adaptive filter, the peak-to-peak value of the rotor displacement is about 15 μm, as shown in Fig. 10(b). After the ISPSO improved VSLMS adaptive filter

compensation, the peak-to-peak value of the rotor displacement is about 7 μm; the rotor vibration is significantly reduced; and the rotor suspension operation is more stable. During operation, the eccentric vibration of the rotor is restrained effectively by the compensation control strategy, and the influence of the eccentricity of the rotor mass is reduced on the operation of the rotor.

In this paper, CCS3.3, an integrated development software widely used in DSP, is used to complete the compilation and operation of ORC-BPMSG. The software VB6.0 is used to develop man-machine interaction interface and realize the online monitoring of experimental data and the online adjustment of the related control parameters.

The main parameters of the ORC-BPMSG in this paper are shown in Table 1, and experiment platform is shown in Fig. 11.

Table 1. Main paramenters of outer rotor coreless bearingless permanent magnet synchronous generator.

Parameters	Values
Rated power	2 kW
Rated speed	3000 r/min
Rotor outer diameter	148 mm
Rotor inner diameter	126 mm
Air gap length	2 mm
Permanent magnet thickness	8 mm
Number of pole pairs of generating winding	3
Number of pole pairs of suspension winding	2
Polar arc coefficient	0.78

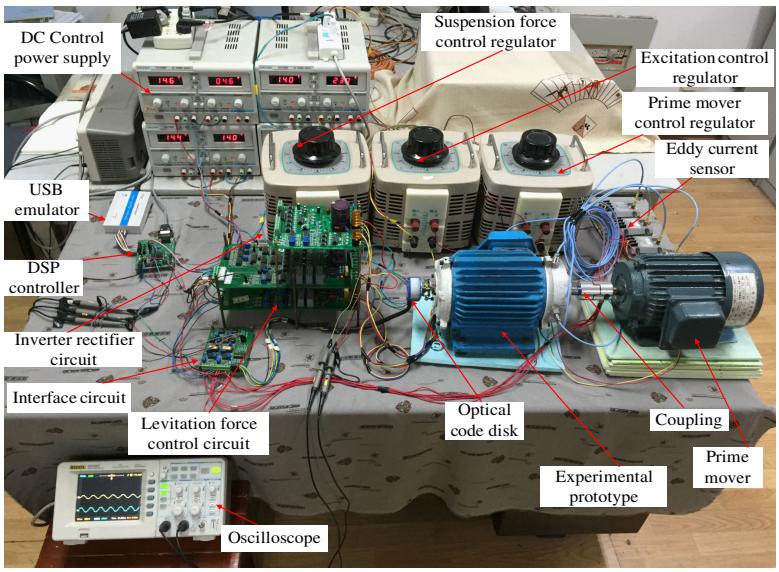

Figure 11. Experiment platform.

5.1. Variable Speed Experiment

The radial displacement curve of the rotor without compensation is shown in Fig. 12(a). When the speed is 2000 r/min, the rotor radial displacement amplitude is about 26 μm, and after 50 ms, when the speed reaches 3000 r/min, the rotor radial displacement amplitude is about 38 μm.

Figure 12(b) shows the radial displacement curve of the rotor after compensation by the variable-step LMS adaptive filter. When the speed is 2000 r/min, the radial displacement amplitude of the rotor is about 14 µm, and the speed reaches 3000 r/min after 50 ms. The radial displacement amplitude of the rotor is about 16 µm. Fig. 12(c) shows the radial displacement curve of the rotor after compensation by the ISPSO improved VSLMS adaptive filter. When the speed is 2000 r/min, the radial displacement amplitude of the rotor is about 6 µm, and when the speed reaches 3000 r/min after 50 ms, the radial displacement amplitude of the rotor is still about 6 µm.

The output voltage curve of the generator without compensation is shown in Fig. 13(a) after the rotor passes through the rectifier circuit. The voltage fluctuates greatly, and the peak-to-peak value of the fluctuation is about 10 V. The output voltage curve of the rotor after compensation is shown in Fig. 13(b) by the ISPSO improved VSLMS adaptive filter. The voltage fluctuation is significantly

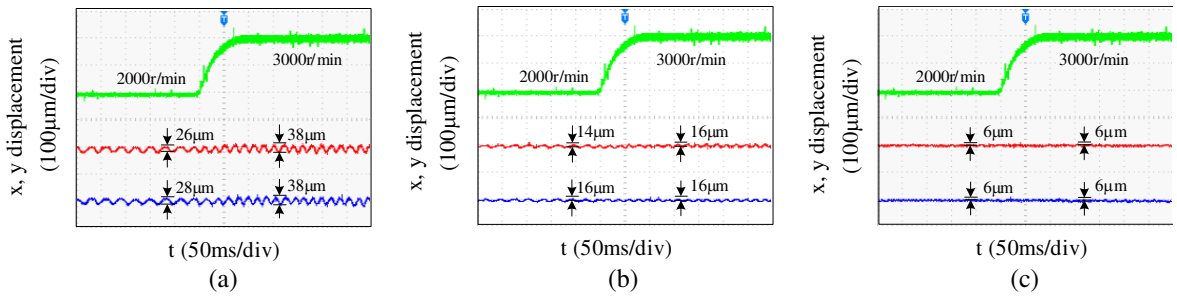

Figure 12. Experiment results of displacement of the rotor under variable speed conditions in the x- and y-direction. (a) Uncompensated displacement. (b) The displacement after VSLMS compensation. (c) The displacement after ISPSO improved VSLMS compensation.

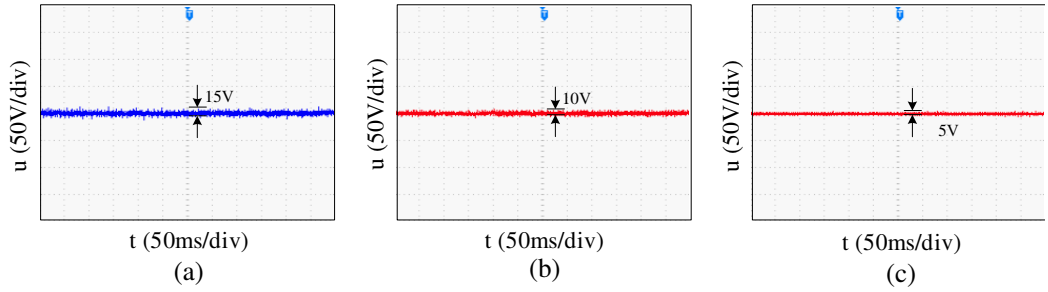

Figure 13. Experiment results of output voltage. (a) Uncompensated output voltage. (b) The output voltage after VSLMS compensation. (c) The output voltage after ISPSO improved VSLMS compensation.

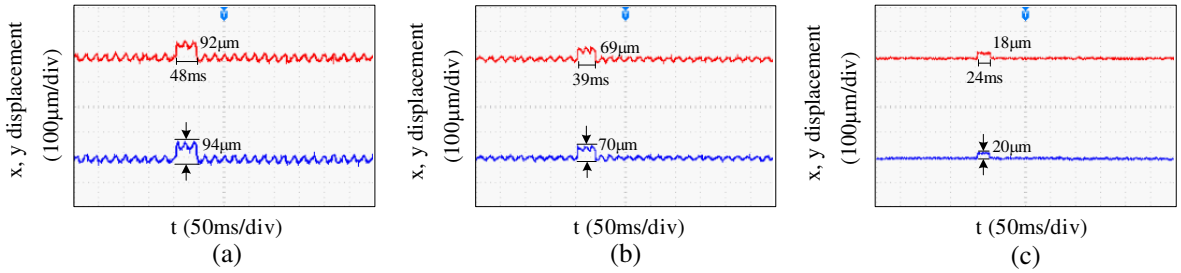

Figure 14. Radial displacement in the x- and y-direction. (a) Uncompensated radial displacement. (b) Radial displacement after VSLMS compensation. (c) Radial displacement after ISPSO improved VSLMS compensation.

reduced, and the peak-to-peak value of the fluctuation is about 5 V. Based on the ISPSO improved VSLMS adaptive filter compensation control strategy proposed in this paper, the stable suspension of the rotor can be realized well, so that the generator can output a stable voltage, thereby ensuring the reliability and stability of the system operation.

Figure 14 shows the displacement waveforms of disturbance test for the proposed method. When motor operates steadily at 3000 r/min, the shaft is suddenly knocked. The maximum displacements are 94 µm and 92 µm in the x- and y-directions without compensation, respectively. The maximum displacements are 70 µm and 69 µm in the x- and y-directions with VSLMS compensation, respectively. The maximum displacements are 20 µm and 18 µm in the x- and y-directions with ISPSO improved VSLMS compensation, respectively. The experimental results show that the proposed ISPSO improved VSLMS compensation has small displacement fluctuation and good anti-interference performance.

6. CONCLUSION

In order to solve the problem of rotor eccentricity caused by rotor mass eccentricity, an improved variable-step LMS adaptive notch filter optimized based on the ISPSO algorithm to realize rotor vibration compensation is proposed in this paper, which effectively suppresses the unbalanced vibration of the rotor and has the following in conclusion:

Due to the rotor eccentricity, the rotor produces unbalanced force when the ORC-BPMSG is rotating at high speed, which causes rotor vibration, resulting in larger current of radial displacement control loop, affecting the safety of the system.

After the vibration compensation is performed with the optimized LMS adaptive filter based on the ISPSO algorithm, the same frequency signal can be basically eliminated, and the peak-to-peak value of the suspension displacement is significantly reduced. After the speed changes, the rotor vibration amplitude does not change, and the output voltage of the generator is more stable.

REFERENCES

1. He, C. and T. Wu, "Analysis and design of surface permanent magnet synchronous motor and generator," *CES Trans. Electric. Mach. Syst.*, Vol. 3, No. 1, 94–100, Mar. 2019.
2. Jin, F., J. Si, Z. Cheng, P. Su, L. Dong, and G. Qi, "Optimization design of a novel toroidal-winding permanent magnet synchronous generator," *22nd Int. Conf. Electric. Mach. Syst. (ICEMS)*, 1–5, Harbin, China, 2019.
3. Yang, X., D. Patterson, and J. Hudgins, "Permanent magnet generator design and control for large wind turbines," *2012 IEEE Power Electric. Mach. Wind Appl.*, 1–5, Denver, USA, 2012.
4. He, C. and T. Wu, "Analysis and design of surface permanent magnet synchronous motor and generator," *CES Trans. Electric. Mach. Syst.*, Vol. 3, No. 1, 94–100, Mar. 2019.
5. Asama, J., A. Mouri, T. Oiwa, and A. Chiba, "Suspension force investigation for consequent-pole and surface-mounted permanent magnet bearingless motors with concentrated winding," *2015 IEEE Int. Electric Mach. Driv. Conf. (IEMDC)*, 780–785, Coeurd'Alene, ID, USA, 2015.
6. Li, H. and H. Zhu, "Design of bearingless flux-switching permanent magnet motor," *IEEE Trans. Appl. Supercond.*, Vol. 26, No. 4, 1–5, Art no. 5202005, Jun. 2016.
7. Diao, X., H. Zhu, Y. Qin, and Y. Hua, "Torque ripple minimization for bearingless synchronous reluctance motor," *IEEE Trans. Appl. Supercond.*, Vol. 28, No. 3, 1–5, Art no. 5205505, Apr. 2018.
8. Zhu, H. and Y. Xu, "Permanent magnet parameter design and performance analysis of bearingless flux switching permanent magnet motor," *IEEE Trans. Ind. Electron.*, Vol. 68, No. 5, 4153–4163, May 2021.
9. Tan, C., H. Wang, and Y. Wang, "Rotor eccentricity compensation of bearingless switched reluctance motors based on extended kalman filter," *2019 12th Int. Symp. Comput. Intell. Des. (ISCID)*, 111–115, Hangzhou, China, 2019.
10. Ye, X. and Z. Yang, "Development of bearingless induction motors and key technologies," *IEEE Access*, Vol. 7, 121055–121066, 2019.

11. Zhu, H. and Y. Hu, "Research on operation principle and control of novel hybrid excitation bearingless permanent magnet generator," *Energies*, Vol. 9, No. 9, 673–689, Sep. 2016.
12. Zhao, H. and C. Zhu, "Feedforward decoupling control for rigid rotor system of active magnetically suspended high-speed motors" *IET Electr. Power Appl.*, Vol. 13, No. 9, 1298–1309, Sep. 2019.
13. Chuan, M. and Z. Changsheng, "Unbalance compensation for active magnetic bearing rotor system using a variable step size real-time iterative seeking algorithm," *IEEE Trans. Ind. Electron.*, Vol. 65, No. 5, 4177–4186, May 2018.
14. Chen, Q., G. Liu, and B. Han, "Suppression of imbalance vibration in AMB-rotor systems using adaptive frequency estimator," *IEEE Trans. Ind. Electron.*, Vol. 62, No. 12, 7696–7705, Dec. 2015.
15. Zhu, H., Z. Yang, X. Sun, D. Wang, and X. Chen, "Rotor vibration control of a bearingless induction motor based on unbalanced force feed-forward compensation and current compensation," *IEEE Access*, Vol. 8, 12988–12998, 2020.
16. Zhao, C., H. Zhu, Y. Du, J. Ju, and Y. Qin, "A novel bearingless flux-switching permanent magnet motor," *2016 IEEE Veh. Power Propuls. Conf. (VPPC)*, 1–5, Hangzhou, China, 2016.